Research Article
Journal of Advanced Development in Engineering and Science
Vol. 13 ● No. 37 • May - August 2023

Temperature–Dependent Penetration Depth of Anisotropic Magnetic Superconductors

Suppanyou Meakniti[1*] and Pongkaew Udomsamuthirun[1]

Recived: 15 May 2023
Revised: 15 June 2023
Accepted: 18 June 2023

ABSTRACT

This research employed a two-band Ginzburg-Landau method to study the temperature- and anisotropic-dependent penetration depth in magnetic superconductors. After calculating the 2nd Ginzburg-Landau equation, we obtain the penetration depth using four temperature-dependent functions proposed by Chen et al., Zhu et al., Shanenko et al., and Changjan and Udomsamuthirun. We also considered two anisotropic functions proposed by Hass and Maki in ellipse shape and Posazhennikova in pancake shape, resulting in 64 possible cross-temperature- and anisotropic-dependent functions. We found that the temperature dependence by Changjan and Udomsamuthirun in the second band, along with pancake and ellipsoidal shapes in the first and second bands (M14-p-e, M24-p-e, M34-p-e, and M44-p-e) provided the best fit with experimental data of the FeCo superconductor.

Keywords: Temperature-dependent; Penetration depth; Anisotropic superconductors; Ginzburg-Landau theory

[1]Prasarnmit Physics Research Unit, Department of Physics, Faculty of Science, Srinakharinwirot University, Bangkok, Thailand 10110
*Corresponding author e-mail: suppanyou.fern@gmail.com

Introduction

A superconductor is a material that exhibits zero electrical resistance and expels magnetic fields, allowing electric currents to flow through it without any energy loss. This phenomenon occurs when the material is cooled below a critical temperature (T_c). At this temperature, the superconductor undergoes a phase transition and enters a state of superconductivity. The critical temperature (T_c), critical current (J_c), and critical magnetic field (H_c) are key properties of a superconductor's phase transition. There are two types of superconductors: Type I and Type II [1]. Type I superconductors are characterized by a sharp transition to the superconducting state and are only effective at low magnetic fields because they have only one critical magnetic field, known as Hc. When the external magnetic field exceeds Hc, the superconductor immediately loses its superconductivity. On the other hand, Type II superconductors have a more gradual transition and can withstand higher magnetic fields because they have two critical magnetic fields, known as lower critical magnetic field (H_{c1}) and upper critical magnetic field (H_{c2}). When the external magnetic field is between H_{c1} and H_{c2}, the magnetic flux can penetrate the superconducting material, but the material still remains in a superconducting state. Only when the magnetic field exceeds H_{c2} does the superconductor lose its superconductivity. This property makes Type II superconductors more suitable for practical applications. When the external magnetic field is below Hc in Type I superconductors and below H_{c1} in Type II superconductors, the superconductor enters a completely superconducting state known as the Meissner effect. In this state, the superconductor exhibits perfect diamagnetism, which expels any magnetic flux from its interior, as proposed by Meissner and Ochsenfeld [2]. When the external magnetic field is between H_{c1} and H_{c2} in Type II superconductors, the superconductor enters a mixed state known as the vortex state, magnetic flux can pass through a superconductor in part. In this state, vortices of normal material form in the superconducting material, and the superconductor exhibits a mixed state between the superconducting and normal states. F. London and H. London [1,3] conducted a study on the penetration of magnetic fields in superconductors, which led to the proposed London penetration depth equation. The Ginzburg-Landau theory [1, 4-5] is a widely accepted theoretical framework used to explain superconductivity in the presence of a magnetic field. In the study of magnetic superconductors based on the Ginzburg-Landau theory, the magnetic free energy proposed by [6-7] is utilized. The Ginzburg-Landau theory's magnetic free energy was employed in researching the surface critical magnetic field [8-12] to understand surface magnetic characteristics. These findings can serve as a reference for thin-film superconductor production and efficiency improvement. Changjan and Udomsamuthirun [13] studied the London penetration depth using magnetic free energy to explain the magnetic penetration of an iron-based superconductor. Askerzade [14] explained the penetration depth in MgB_2 using the two-band Ginzburg-Landau theory of the superconductor. Tongkhonburi and

Udomsamuthirun [15] investigated the penetration depth of MgB_2 and CaAlSi using the two-band Ginzburg-Landau theory. They considered anisotropy with ellipse and pancake shapes to explain the band structure of the materials. The measurement of penetration depth is an effective means of studying multi-band superconductivity, as demonstrated by Prozorov and Kogan [16]. Their findings have provided valuable insights into the behavior of iron-based superconductors. In this research, we investigate the penetration depth of two-band magnetic superconductors using four temperature-dependent assumptions [17] and two anisotropic functions [18–19]. Our analysis considers the cross between the first and second bands, the temperature, and the anisotropic cross, and compares the results obtained from our calculations with the experimental data obtained from FeCo superconductor measurements [16]. FeCo is a tetragonal iron-based superconductor with a high critical temperature (T_c), depending on its composition. It is known for its anisotropic superconducting properties, with higher critical current density in the ab plane than along the c-axis. It is also a well-known magnetic material with the highest saturation magnetization among various transition metal alloys [20]. The electronic structure determines the energy levels and band structure of materials. Anisotropic penetration depth arises from electronic structure anisotropy, such as variations in energy bands along crystallographic directions. This influences the density of states, impacting the anisotropic behavior of the penetration depth. The electronic structure of the iron-based superconductor is described in Ref. [21]. The superexchange interactions create magnetic correlations and impact the pairing mechanism. The anisotropic nature of superexchange, determined by crystal structure and magnetic moment arrangement, introduces anisotropic spin fluctuations that influence the anisotropic behavior of the penetration depth. The superexchange mechanism of high critical temperature superconductivity is described in Ref. [22]. The charge-transfer gap influences the pairing mechanism and nature of superconductivity. Anisotropic variations in the charge-transfer gap affect the electronic density of states, Fermi surface topology, and electron-phonon interactions, contributing to anisotropic penetration depth. The charge-transfer gap of high critical temperature superconductors is described in Ref. [23].

Model and Calculation

The penetration depth for magnetic superconductors can be determined by employing anisotropic two-band free energy using the Ginzburg-Landau theory. This has been explored in previous studies [6-7]. Our focus is on investigating the anisotropy and temperature dependence of this free energy. The expression for two-band free energy as

$$F_{sc}\left[\psi_1,\psi_2\right]=\int d^3r\left(f_1+f_2+f_{12}+\gamma_0+\gamma_1 B+\gamma_2\frac{B^2}{2\mu_0}\right) \quad (1)$$

$$F_{i(i=1,2)} = \frac{1}{2m_i}\left|\left(-i\hbar\nabla - 2e\vec{A}\right)\psi_i\right|^2 \left\langle f_i^2\left(\hat{k}\right)\right\rangle$$

$$+\alpha_i(T)\psi_i^2\left\langle f_i^2\left(\hat{k}\right)\right\rangle + \frac{1}{2}\beta_i\psi_i^4\left\langle f_i^2\left(\hat{k}\right)\right\rangle \quad (2)$$

$$F_{12} = \varepsilon\left(\psi_1^*\psi_2 + c.c\right)\left\langle f_1\left(\hat{k}\right)f_2\left(\hat{k}\right)\right\rangle$$

$$+\varepsilon_1\left\{\left(i\hbar\nabla - 2e\vec{A}\right)\psi_1^*\left(-i\hbar\nabla - 2e\vec{A}\right)\psi_2 + c.c.\right\}\left\langle f_1\left(\hat{k}\right)f_2\left(\hat{k}\right)\right\rangle \quad (3)$$

The anisotropic free energy of each band is referred to as F_i ,and the interaction between the first and second bands is represented by F_{12} . F_i is made up of three parts: the kinetic energy, the temperature-dependent part, and the temperature-independent part. The effective mass of electron carriers is represented by m_i. The order parameter is denoted by ψ_i . The coefficients α_i and β_i correspond to temperature-dependent and temperature-independent properties, respectively. The anisotropic function $f_i(\hat{k})$ is defined, with the variables of the first and second bands represented by the subscripts $i(i=1,2)$. This function has been discussed by [18-19]. The interaction between the two order parameters and their gradient is represented by ε and ε_1 . The complex conjugate is abbreviated as $c.c.$. The vector potential is represented by $\vec{A}$,and the magnetic field is given as a series of $\gamma_0 + \gamma_1 B + \gamma_2 \frac{B^2}{2\mu_0}$,where γ_0, γ_1, and γ_2 are coefficients of the magnetic field series, which [6-7] have discussed. By applying the Ginzburg-Landau approach, we can obtain the 1st Ginzburg-Landau equation as equations (4) and (5) by taking the variation equation (1) with respect to ψ_1^* and ψ_2^* , and derive the 2nd Ginzburg-Landau as equation (6) by taking the variation equation (1) with respect to $\vec{A}$ [24-25].

$$\frac{\left\langle f_1^2\left(\hat{k}\right)\right\rangle}{2m_1}\left(-i\hbar\vec{\nabla} - 2e\vec{A}\right)^2\psi_1 + \alpha_1\left\langle f_1^2\left(\hat{k}\right)\right\rangle\psi_1 + \varepsilon\left\langle f_1\left(\hat{k}\right)f_2\left(\hat{k}\right)\right\rangle\psi_2$$

$$+\varepsilon_1\left\langle f_1\left(\hat{k}\right)f_2\left(\hat{k}\right)\right\rangle\left(-i\hbar\vec{\nabla} - 2e\vec{A}\right)^2\psi_2 = 0 \quad (4)$$

$$\frac{\left\langle f_2^2\left(\hat{k}\right)\right\rangle}{2m_2}\left(-i\hbar\vec{\nabla}-2e\vec{A}\right)^2\psi_2+\alpha_2\left\langle f_2^2\left(\hat{k}\right)\right\rangle\psi_2+\varepsilon\left\langle f_1\left(\hat{k}\right)f_2\left(\hat{k}\right)\right\rangle\psi_1$$

$$+\varepsilon_1\left\langle f_1\left(\hat{k}\right)f_2\left(\hat{k}\right)\right\rangle\left(-i\hbar\vec{\nabla}-2e\vec{A}\right)^2\psi_1=0 \quad (5)$$

$$-\left(\frac{\gamma_1}{B}+\frac{\gamma_2}{\mu_0}\right)\mu_0\vec{\nabla}\times(1+\chi')M_{sc}=\frac{\left\langle f_1^2(\hat{k})\right\rangle}{2m_1}\left[2ie\hbar(\psi_1^*\vec{\nabla}\psi_1-\psi_1\vec{\nabla}\psi_1^*)+8e^2A\left|\psi_1\right|^2\right]$$

$$+\frac{\left\langle f_2^2(\hat{k})\right\rangle}{2m_2}\left[2ie\hbar(\psi_2^*\vec{\nabla}\psi_2-\psi_2\vec{\nabla}\psi_2^*)+8e^2A\left|\psi_2\right|^2\right]$$

$$+\varepsilon_1\left\langle f_1(\hat{k})f_2(\hat{k})\right\rangle\begin{bmatrix}2ie\hbar(\psi_1^*\vec{\nabla}\psi_2-\psi_2\vec{\nabla}\psi_1^*)+8e^2A\psi_1^*\psi_2\\+2ie\hbar(\psi_2^*\vec{\nabla}\psi_1-\psi_1\vec{\nabla}\psi_2^*)+8e^2A\psi_2^*\psi_1\end{bmatrix} \quad (6)$$

Where μ_0 is the magnetic permeability, χ and χ' are the magnetic susceptibility and differential magnetic susceptibility, respectively, and M_{sc} is the magnetization. We have the solution for the wave function as $\psi=\left|\psi\right|e^{i\phi}$, ϕ is the phases of order parameter. When $\vec{\nabla}\times M_{sc}=J_{sc}$, we can apply Maxwell's equation $J=\vec{\nabla}\times\vec{B}$ to obtain a related expression.

$$\frac{d^2\vec{B}(x)}{dx^2}-\frac{1}{-\gamma_2(1+\chi')}\begin{bmatrix}\frac{\left\langle f_1^2(\hat{k})\right\rangle}{2m_1}8e^2\left|\psi_1\right|^2+\frac{\left\langle f_2^2(\hat{k})\right\rangle}{2m_2}8e^2\left|\psi_2\right|^2\\+\varepsilon_1\left\langle f_1(\hat{k})f_2(\hat{k})\right\rangle 8e^2(\psi_1^*\psi_2+\psi_2^*\psi_1)\end{bmatrix}\vec{B}=0 \quad (7)$$

Equations (4) and (5) can be used to calculate the equilibrium value of the order parameter in the absence of a magnetic field in equations (8) and (9).

$$\left|\psi_1\right|^2=\frac{\alpha_1\left\langle f_1^2(k)\right\rangle+\frac{\varepsilon\left\langle f_1(k)f_2(k)\right\rangle}{\theta}}{\beta_1} \quad (8)$$

$$\left|\psi_2\right|^2=\frac{\alpha_2\left\langle f_2^2(k)\right\rangle+\varepsilon\left\langle f_1(k)f_2(k)\right\rangle\theta}{\beta_2} \quad (9)$$

Equation (7) can be compared with the London equation: $\frac{d^2\vec{B}(x)}{dx^2}-\frac{1}{\lambda^2}\vec{B}(x)=0$, λ is the London penetration depth, which describes a temperature-dependent penetration depth that exhibits anisotropic behavior in equation (10)

$$\frac{1}{\lambda^2}=\frac{4e^2}{\gamma_2(1+\chi')m_1}\left[\frac{\alpha_1\langle f_1^2(k)\rangle+\frac{\varepsilon\langle f_1(k)f_2(k)\rangle}{\theta}}{\beta_1}\right]+\frac{4e^2}{\gamma_2(1+\chi')m_2}\left[\frac{\alpha_2\langle f_2^2(k)\rangle+\varepsilon\langle f_1(k)f_2(k)\rangle\theta}{\beta_2}\right]+16e^2\varepsilon_1\left\langle f_1(\hat{k})f_2(\hat{k})\right\rangle\left[\begin{array}{c}\left(\frac{\alpha_1\langle f_1^2(k)\rangle+\frac{\varepsilon\langle f_1(k)f_2(k)\rangle}{\theta}}{\beta_1}\right)^{\frac{1}{2}}\\ \left(\frac{\alpha_2\langle f_2^2(k)\rangle+\varepsilon\langle f_1(k)f_2(k)\rangle\theta}{\beta_2}\right)^{\frac{1}{2}}\end{array}\right] \quad (10)$$

We use four temperature dependency models [17], including M1: $\alpha_{ch}=\left(1-\frac{T}{T_c}\right)$ [26], M2: $\alpha_{Zh}=\left(1-\left(\frac{T}{T_c}\right)^2\Big/1+\left(\frac{T}{T_c}\right)^2\right)$ [27], M3: $\alpha_{Sh}=\left(1-\frac{T}{T_c}\right)+\frac{1}{2}\left(1-\frac{T}{T_c}\right)^2$ [28], and M4: $\alpha_{Ud}=p\left(1-\frac{T}{T_c}\right)+\frac{q}{2}\left(1-\frac{T}{T_c}\right)^2$ [17], and two anisotropic functions of ellipse and pancake shape [18-19]. The Hass and Maki model proposes an anisotropic function in the shape of an ellipse, $f(\theta)=\frac{1+a\cos^2\theta}{1+a}$, Similarly, Posazhennikova's model adopts a pancake shape, $f(\theta)=\frac{1}{\sqrt{1+b\cos^2\theta}}$, where the constant a and b determines the level of anisotropy and θ represents the azimuthal angle. Our model incorporates 64 events of temperature dependence and anisotropy. These events result from the crossover between the first and second bands of four temperature-dependent functions and two anisotropic functions of the two-band superconductor.

Results and Discussion

Upon performing the calculations, it was determined that solely the terms associated with M4 yielded outcomes that were in close agreement with the FeCo [16] experimental findings. The FeCo 122 crystal is an iron-based superconductor that has a tetragonal structure. It is also a magnetic material with a body-centered cubic (bcc) structure that is widely recognized for having the highest saturation magnetization (Ms) and T_c values among transition metal alloys [20]. The critical temperature (T_c) of this material for superconductivity is relatively high and varies depending on its specific composition. It is anisotropic in its superconducting properties and has a greater critical current density in the ab plane than along the c-axis. To present the numerical outcomes, we will solely employ the combinations M1-M4 (M14), M2-M4 (M24), M3-M4 (M34), and M4-M4 (M44). Figures 1-4 show the cross-temperature dependence and anisotropy on penetration depths M14, M24, M34, and M44 as functions of λ (penetration depth) and T (temperature). The cross-model of M14 shown in Figure 1-(A) and -(B), in c-axis set to $\theta = 0.5$, when M14-e-e: $a = 0.5$, $b = 0.5$, M14-e-p: $a = 0.5$, $b = 40$, M14-p-e: $a = 40$, $b = 0.5$ and M14-p-p: $a = 40$, $b = 5$, in ab-plane set to $\theta = 5$, when M14-e-e: $a = 0.1$, $b = 0.1$, M14-e-p: $a = 0.1$, $b = 1$, M14-p-e: $a = 1$, $b = 0.1$ and M14-p-p: $a = 1$, $b = 1$.The cross-model of M24 shown in Figure 2-(A) and -(B), in c-axis set to $\theta = 0.5$, when M24-e-e: $a = 0.5$, $b = 0.5$, M24-e-p: $a = 0.5$, $b = 40$, M24-p-e: $a = 40$, $b = 0.5$ and M24-p-p: $a = 40$, $b = 5$, in ab-plane set to $\theta = 0.5$, when M24-e-e: $a = 0.1$, $b = 0.1$, M24-e-p: $a = 0.1$, $b = 1$, M24-p-e: $a = 1$, $b = 0.1$ and M24-p-p: $a = 1$, $b = 1$. The cross-model of M34 shown in Figure 3-(A) and -(B), in c-axis set to $\theta = 0.5$, when M34-e-e: $a = 0.5$, $b = 0.5$, M34-e-p: $a = 0.5$, $b = 40$, M34-p-e: $a = 40$, $b = 0.5$ and M34-p-p: $a = 40$, $b = 5$, in ab-plane set to $\theta = 5$, when M34-e-e: $a = 0.1$, $b = 0.1$, M34-e-p: $a = 0.1$, $b = 1$, M34-p-e: $a = 1$, $b = 0.1$ and M34-p-p: $a = 1$, $b = 1$. The cross-model of M44 shown in Figure 4-(A) and -(B), in c-axis set to $\theta = 0.5$, when M44-e-e: $a = 0.5$, $b = 0.5$, M44-e-p: $a = 0.5$, $b = 40$, M44-p-e: $a = 40$, $b = 0.5$ and M44-p-p: $a = 40$, $b = 5$, in ab-plane set to $\theta = 5$, when M44-e-e: $a = 0.1$, $b = 0.1$, M44-e-p: $a = 0.1$, $b = 1$, M44-p-e: $a = 1$, $b = 0.1$ and M44-p-p: $a = 1$, $b = 1$.

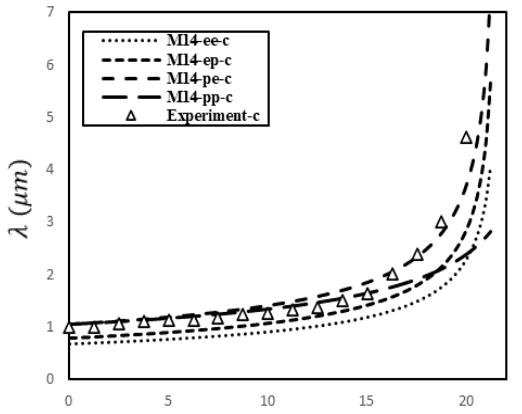

(A) in c-axis

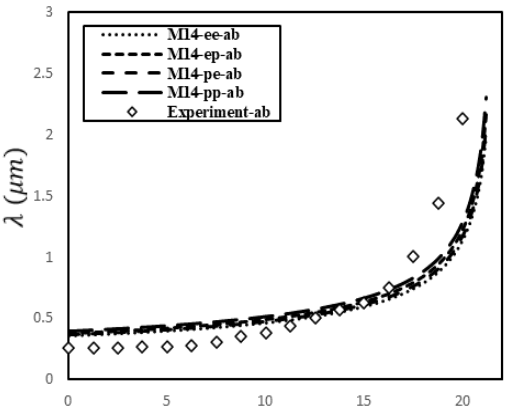

(B) in ab-plane

Figure 1 Shows the relationship between penetration depth and temperature of M14

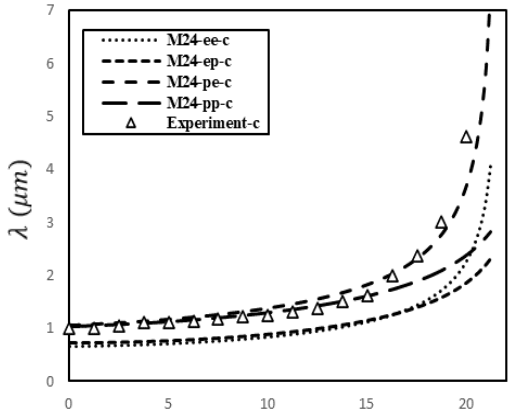

(A) in c-axis

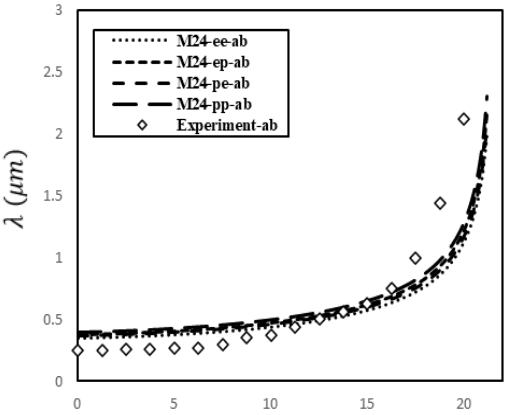

(B) in ab-plane

Figure 2 Shows the relationship between penetration depth and temperature of M24

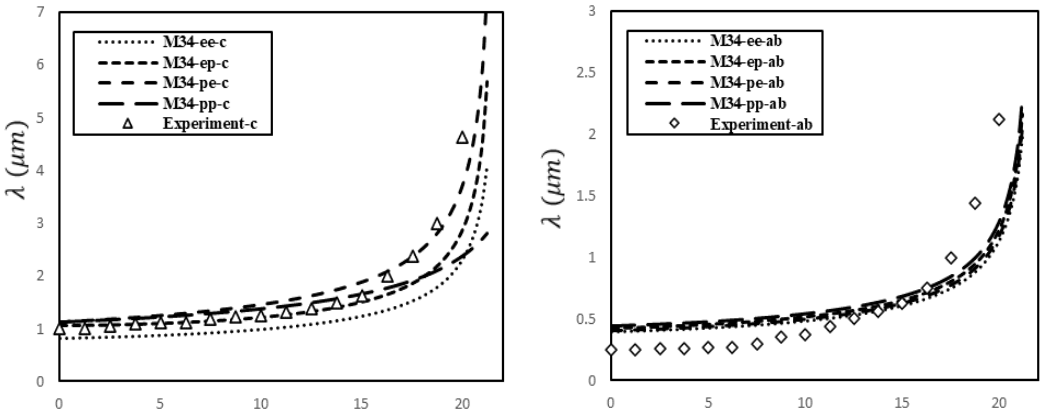

(A) in c-axis (B) in ab-plane

Figure 3 Shows the relationship between penetration depth and temperature of M34

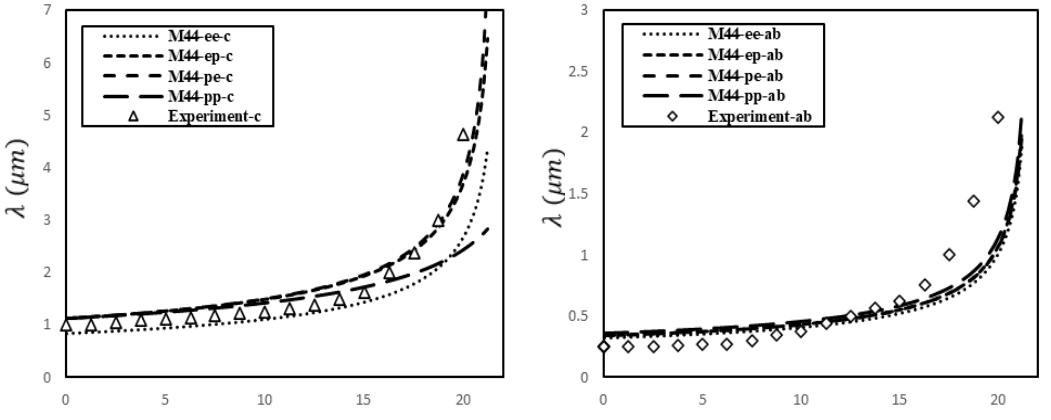

(A) in c-axis (B) in ab-plane

Figure 4 Shows the relationship between penetration depth and temperature of M44

We examined 64 different models of cross-temperature-dependent and cross-anisotropic functions between bands 1 and 2. We classified the temperature dependence into four cases, each involving four different cases: Case 1 (M11, M12, M13, and M14); Case 2 (M21, M22, M23, and M24); Case 3 (M31, M32, M33, and M34); and Case 4 (M41, M42, M43, and M44). For each case, we calculated the anisotropic functions for ellipse-ellipse (e-e), ellipse-pancake (e-p), pancake-ellipse (p-e), and pancake-pancake (p-p), resulting in a total of 64 considered models. Our analysis showed that utilizing the temperature function developed by Changjan and Udomsamuhiran [17] in the second band of all cases, along

with the pancake-shaped in the first band and the ellipsoidal shapes in the second band (M14-p-e, M24-p-e, M34-p-e, and M44-p-e), produced results consistent with FeCo's experimental results [16]. This was true for both the in-ab-plane (FeCo-ab) and c-axis (FeCo-c), which were relatively stable near zero Kelvin and rapidly increased at critical temperatures as shown in Figure 5. This indicates that the magnetic field can penetrate into the superconductor until a certain point, where the magnetic field becomes so high that it can destroy the superconductivity.

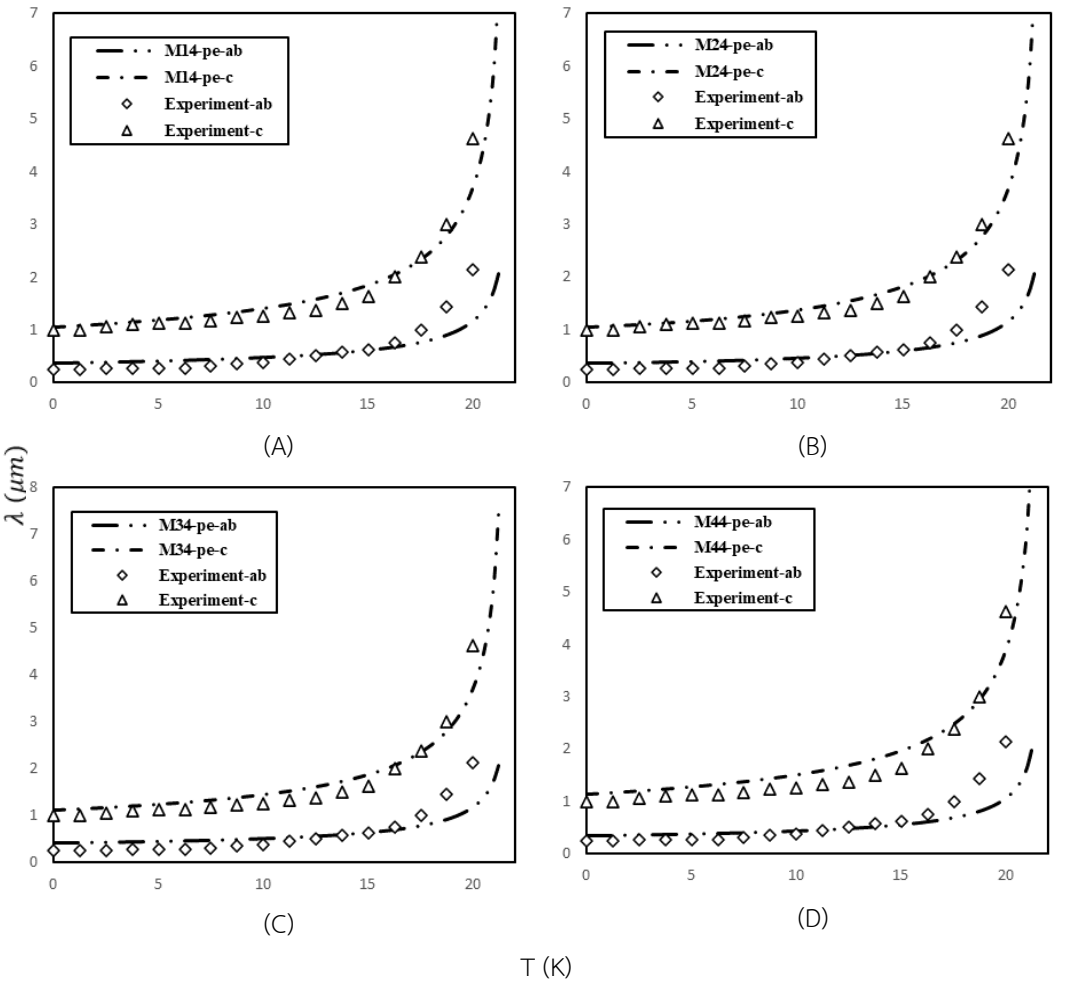

Figure 5 Shows the relationship between in c-axis and ab-plane versus T of cross-temperature-dependent for (A) M14, (B) M24, (C) M34 and (D) M44.

Conclusions

Our research focused on the study of the penetration depth of anisotropic two-band magnetic superconductors. To achieve this, we applied the Ginzburg-Landau theory and began by calculating the penetration depth using the anisotropic two-band free energy equation. We then obtained the second Ginzburg-Landau equation by minimizing the free energy with respect to the vector potential. We modify the 2^{nd} Ginzburg-Landau equation using Maxwell's equations to obtain the two-band penetration depth that is both temperature- and anisotropic-dependent, which can be reduced to a one-band penetration depth equation. The results of the temperature dependence and the anisotropic dependence of the penetration depth were analyzed by a trial method using four temperature-dependent functions and two anisotropic functions. We explored 64 models of cross-temperature-dependent and cross-anisotropic functions between the first and second bands, resulting in 64 models. Our analysis found that using the temperature function developed by Changjan and Udomsamuhiran [17] in the second band for all cases and pancake-shaped in the first band and ellipsoidal shapes in the second band (M14-p-e, M24-p-e, M34-p-e, and M44-p-e) produced consistent results with experimental data of FeCo in both the in-ab-plane and c-axis [16]. This discovery of the band structure shape, particularly the Fermi surface form of penetration depth in magnetic superconductors, has significant implications for researchers.

Acknowledgments

Our wish is to acknowledge the encouragement from Prasarnmit Physics Research Unit, Department of Physics, Faculty of Science, Srinakharinwirot University, and the financial support from the Royal Golden Jubilee Ph.D. Programme (Grant No. PHD/0212/2561) through the National Research Council of Thailand (NRCT) and Thailand Research Fund (TRF).

References

[1] Kittel, C., & McEuen, P. (2018). Introduction to solid state physics. Hoboken, NJ: John Wiley & Sons.

[2] Ketterson, J. B., Ketterson, J. B., & Song, S. N. (1999). *Superconductivity*. Cambridge: Cambridge University Press.

[3] London, F., & London, H. (1935). The electromagnetic equations of the supraconductor. *Proceedings of the Royal Society of London. Series A-Mathematical and Physical Sciences*, 149(866), 71-88.

[4] Buckel, W. (1991). *Superconductivity: Fundamentals and Applications*. Weinheim:

Wiley-VCH.

[5] Poulter, J. (1991). *Lectures on Ginzburg-Landau (GL) Theory in The Theory of Superconductivity*. Bangkok: Faculty of Science, Chulalongkorn University.

[6] Hampshire, D. P. (1998). Ferromagnetic and antiferromagnetic superconductivity. *Physica C: Superconductivity and its Applications*, 304(1-2), 1-11.

[7] Hampshire, D. P. (2001). The non-hexagonal flux-line lattice in superconductors. *Journal of Physics: Condensed Matter*, 13(27), 6095.

[8] Meakniti, S., et al. (2014). The study on surface critical magnetic field of a layered magnetic superconductors. *Advanced Materials Research*, 979, 224-227

[9] Changjan, A., et al. (2017). The temperature-dependent surface critical magnetic field (H_{C3}) of magnetic superconductors: Applied to lead bismuth ($Pb_{82}Bi_{18}$) superconductors. *Journal of Physics and Chemistry of Solids*, 107, 32-35.

[10] Meakniti, S., et al. (2023). The temperature dependent surface critical magnetic field (H_{c3}) of $K_{0.73}Fe_{1.68}Se_2$ superconductor by semi-anisotropic two band Ginzburg-Landau approach. *Journal of Physics: Conference Series*, 2431, 012044.

[11] Meakniti, S., et al. (2023). A Study of the Temperature-Dependent Surface and Upper Critical Magnetic Fields in KFeSe and LaSrCuOSuperconductors. *Crystals*, 13(3), 526.

[12] Maksuwan, A., et al. (2023). The third critical field (H_{c3}) of single-crystalline $K_{0.73}Fe_{1.68}Se_2$ by ginzburg-landau approach. *Suranaree Journal of Science and Technology*, 30(2), 010208.

[13] Changjan, A., &Udomsamuthirun, P. (2014). London penetration depth of Fe-based superconductors. *Advanced Materials Research*, 979, 297-301.

[14] Askerzade, I. N., &Gencer, A. (2002). London penetration depth λ (T) in two-band Ginzburg–Landau theory: application to MgB_2. *Solid state communications*, 123(1-2), 63-67.

[15] Tongkhonburi, P., & Udomsamuthirun, P. (2019). The study on penetration depth of anisotropic two-band superconductors by Ginzburg–Landau approach. *Physica C: Superconductivity and its Applications*, 561, 45-48.

[16] Prozorov, R., & Kogan, V. G. (2011). London penetration depth in iron-based superconductors. *Reports on Progress in Physics*, 74(12), 124505.

[17] Changjan, A., & Udomsamuthirun, P. (2013). Critical temperature of magnetic superconductors by two-band Ginzburg-Landau approach. *Songklanakarin Journal of Science & Technology*, 35(5).

[18] Haas, S., & Maki, K. (2001). Anisotropic s-wave superconductivity in MgB_2. *Physical Review B*, 65(2), 020502.

[19] Posazhennikova, A. I., et al. (2002). Anisotropic s-wave superconductivity: Comparison with experiments on MgB_2 single crystals. *Europhysics Letters*, 60(1), 134.

[20] Hasegawa, T., et al. (2019). Stabilisation of tetragonal FeCo structure with high magnetic anisotropy by the addition of V and N elements. *Scientific Reports*, 9(1), 5248.

[21] Lu, D. H., et al. (2008). Electronic structure of the iron-based superconductor LaOFeP. *Nature*, 455(7209), 81-84.

[22] Ruckenstein, A. E., et al. (1987). Mean-field theory of high-T_c superconductivity: The superexchange mechanism. *Physical Review B*, 36(1), 857.

[23] Jarrell, M., et al. (1988). Charge-transfer mechanisms for high-T_c superconductivity. *Physical Review B*, 38(7), 4584.

[24] Changjan, A., & Udomsamuthirun, P. (2011). Critical magnetic field ratio of anisotropic magnetic superconductors. *Physica C: Superconductivity and its Applications*, 471(1-2), 23-25.

[25] Changjan, A., & Udomsamuthirun, P. (2011). The critical magnetic field of anisotropic two-band magnetic superconductors. *Solid State Communications*, 151(14-15), 988-992.

[26] Chen, L., et al. (2011). Two-band calculations on the upper critical field of superconductor $NbSe_2$. *Physica C: Superconductivity and its Applications*, 471(23-24), 1591-1594.

[27] Zhu, X., et al. (2008). Upper critical field, Hall effect and magnetoresistance in the iron-based layered superconductor $LaFeAsO_{0.9}F_{0.1-\delta}$. *Superconductor Science and Technology*, 21(10), 105001.

[28] Shanenko, A., et al. (2011). Extended Ginzburg-Landau formalism for two-band superconductors. *Physical review letters*, 106(4), 047005.